Biosensors and Bioelectronics 102 (2018) 372–382

Contents lists available at ScienceDirect

Biosensors and Bioelectronics

journal homepage: www.elsevier.com/locate/bios

Selective isolation and noninvasive analysis of circulating cancer stem cells through Raman imaging

Hyeon-Yeol Cho[a,b,1], Md. Khaled Hossain[c,1], Jin-Ho Lee[a,b], Jiyou Han[d], Hun Joo Lee[c,e], Kyeong-Jun Kim[a], Jong-Hoon Kim[f], Ki-Bum Lee[b,*,2], Jeong-Woo Choi[a,c,**,3]

[a] Department of Chemical and Biomolecular Engineering, Sogang University, Seoul 04107, South Korea
[b] Department of Chemistry and Chemical Biology, Rutgers, The State University of New Jersey, Piscataway, NJ 08854, USA
[c] Interdisciplinary Program of Integrated Biotechnology, Sogang University, Seoul 04107, South Korea
[d] Department of Biological Sciences, Laboratory of Stem Cell Research and Biotechnology, Hyupsung University, Hwasung-si 18330, South Korea
[e] DP Team, Samsung Bioepis, Incheon 21987, South Korea
[f] Department of Biotechnology, Laboratory of Stem Cells and Tissue Regeneration, College of Life Sciences and Biotechnology, Korea University, Seoul 02841, South Korea

ARTICLE INFO

Keywords:
Circulating cancer stem cells
Metastasis
Circulating tumor cells
Raman-active nanoprobes
Raman imaging

ABSTRACT

Circulating cancer stem cells (CCSCs), a rare circulating tumor cell (CTC) type, recently arose as a useful resource for monitoring and characterizing both cancers and their metastatic derivatives. However, due to the scarcity of CCSCs among hematologic cells in the blood and the complexity of the phenotype confirmation process, CCSC research can be extremely challenging. Hence, we report a nanoparticle-mediated Raman imaging method for CCSC characterization which profiles CCSCs based on their surface marker expression phenotypes. We have developed an integrated combinatorial Raman-Active Nanoprobe (RAN) system combined with a microfluidic chip to successfully process complete blood samples. CCSCs and CTCs were detected (90% efficiency) and classified in accordance with their respective surface marker expression *via* completely distinct Raman signals of RANs. Selectively isolated CCSCs (93% accuracy) were employed for both *in vitro* and *in vivo* tumor phenotyping to identify the tumorigenicity of the CCSCs. We utilized our new method to predict metastasis by screening blood samples from xenograft models, showing that upon CCSC detection, all subjects exhibited liver metastasis. Having highly efficient detection and noninvasive isolation capabilities, we have demonstrated that our RAN-based Raman imaging method will be valuable for predicting cancer metastasis and relapse *via* CCSC detection. Moreover, the exclusion of peak overlapping in CCSC analysis with our Raman imaging method will allow to expand the RAN families for various cancer types, therefore, increasing therapeutic efficacy by providing detailed molecular features of tumor subtypes.

1. Introduction

Cancer stem cells (CSCs) refer to a small subset of tumor cells that have the unique ability to self-renew and differentiate. Their self-renewal process typically drives tumorigenesis and their differentiation process causes tumor heterogeneity (Jordan et al., 2006; Malanchi et al., 2012). CSCs can be identified by biomarkers showing stem-like characteristics, such as CD133 and CD44, which are responsible for stemness and pleiotropic roles in cell adhesion, migration, and homing (Mizrak et al., 2008; Zöller, 2011). Even though CSCs account for a small fraction of tumor cell population (~1%), they are known to have a critical role in cancer metastasis and relapse owing to their distinctive abilities including self-renewal, differentiation, and chemoresistance (Medema, 2013; Melo et al., 2017; Moncharmont et al., 2012; Pathania et al., 2016; Visvader and Lindeman, 2008). For example, in the metastasis process, metastatic cancer cells, including CSCs, migrate along vasculature in the lymph nodes to initiate tumor growth at secondary organ sites by extravasation (Maheswaran and Haber, 2010; Riethdorf et al., 2008). While it is known that most circulating tumor cells (CTCs) obtain a migratory cell fate and lose epithelial properties through the process of epithelial to mesenchymal transition (EMT), the metastatic process is enormously complex and highly dynamic (Maheswaran and

* Corresponding author at: Department of Chemistry and Chemical Biology, Rutgers, The State University of New Jersey, Piscataway, NJ 08854, USA.
** Corresponding author. Department of Chemical and Biomolecular Engineering, Sogang University, Seoul, 04107, South Korea.
E-mail addresses: kblee@rutgers.edu (K.-B. Lee), jwchoi@sogang.ac.kr (J.-W. Choi).
[1] Equal contribution.
[2] http://kblee.rutgers.edu
[3] http://home.sogang.ac.kr/sites/nbel

https://doi.org/10.1016/j.bios.2017.11.049
Received 28 August 2017; Received in revised form 13 November 2017; Accepted 15 November 2017
Available online 16 November 2017
0956-5663/ © 2017 Elsevier B.V. All rights reserved.

Haber, 2010), thereby the detailed mechanisms underlying CTC migration have not been well studied. Scientists have reported that only a small subset of CTCs, categorized and termed circulating cancer stem cells (CCSCs), are involved in successful cancer metastasis, exhibiting high invasiveness (Cristofanilli et al., 2004; Kennecke et al., 2010; Malanchi et al., 2012). Given these extraordinary characteristics, combined with the important functions of CCSCs have in cancer metastasis, a highly selective detection and analysis method for the isolation of CCSCs from a heterogeneous CTC population is essential for advancing cancer therapeutics and will providing new insights into cancer metastasis and relapse at the single cell levels (Nadal et al., 2013).

Due to the scarcity of CCSCs and CTCs among heterogeneous blood cells, as few as one cell per 10^9 hematologic cells in the blood of patients, simultaneous detection, isolation, and analysis of CCSCs and CTCs in a highly selective, sensitive, and non-invasive manner is extremely challenging (Cristofanilli et al., 2004; Lawson et al., 2015; Nagrath et al., 2007). The fluorescence-activated cell sorting (FACS) method has been utilized for CCSC isolation and detection by comparing a CSC marker (CD133 or CD44) with white blood cell (WBC) marker (CD45) expression (Al-Hajj et al., 2003; Ginestier et al., 2007; Kantara et al., 2015; Lawson et al., 2015; Liu et al., 2014). However, it is limited in validating primary cancer phenotypic characters considering that CSC markers are expressed not only on CSCs but also on normal stem cells (Pattabiraman and Weinberg, 2014). Therefore, it is necessary to combine the CCSC and CTC detection for improving accuracy in CCSC research. For example, detecting and analyzing breast CCSCs and CTCs, which have four subtypes including luminal, human epidermal growth factor receptor 2 (HER2) positive, and two triple-negative types (Basal-A and Basal-B), requires the use of a combination of at least five antibodies (four antibodies for subtyping, epithelial cell adhesion molecule (EpCAM), HER2, human epidermal growth factor receptor 1 (EGFR), and mucin 1 (MUC1), and one antibody for stemness confirmation (CD133)) (Carey et al., 2007; Eirew et al., 2008; Kao et al., 2009; Kennecke et al., 2010; Neve et al., 2006; Perou et al., 2000) (Table 1). Therefore, simultaneous detection and analysis of various subtypes of CCSCs and CTCs, showing primary cancer's heterogeneity *via* a multi-probe-based platform, requires an innovative method for efficient multiplex detection of subpopulations of heterogeneous cancer cells and the analysis of a wide range of complex analytes.

To this end, several CTC detection chips using immune-affinity-based separation methods with multiple fluorescent probes have demonstrated limited success for CCSC detection. (Lee et al., 2013a, 2013b; Yoon et al., 2013). However, given the limitations of the fluorescent probe systems, it is difficult to analyze CTC subtypes with high isolation efficiency from blood, particularly for CCSCs with significantly different quantities which require an increase in the number of probes. This is an especially critical challenge in multicolor analysis, where it is impossible to discriminate between fluorophores that spectrally overlap (Lichtman and Conchello, 2005; Zhang et al., 2016). Therefore, there remains significant room for improvement in achieving highly sensitive and specific cell detection methods that can display broad multiplexing capabilities with high reproducibility.

Raman imaging with surface-enhanced Raman spectroscopy (SERS) has significant advantages when compared to fluorescence imaging, including spectral information that shows a larger number of characteristic peaks, and crucially, distinct non-overlapping peaks. (Papadopoulou and Bell, 2011; Sabatte et al., 2008; Ye et al., 2017; Zhai et al., 2012; Zheng et al., 2012). Particularly, SERS has shown signals with low background noise in biological samples including those drawn from blood by avoiding autofluorescent signals (Premasiri et al., 2012; Wang et al., 2011). These comprehensive advantages render SERS as highly competitive in meeting the needs of multiplex quantification of molecules in living cells. However, to the best of our knowledge, a Raman imaging-based detection and analysis method of CCSC has not yet been reported. To detect and analyze CCSCs, three requirements must be satisfied for CTC research: a high detection yield of target cells in the blood, non-invasive isolation of captured cells, and the simultaneous detection of surface markers with different expression levels.

To address the aforementioned challenges for the detection and downstream analysis of CCSCs and CTCs, we report a novel combinatorial Raman-Active Nanoprobe (RAN)-based chip platform with the capability of simultaneous detection, isolation, and further analysis of CCSCs and various CTC subtypes though Raman imaging (Fig. 1). The RAN is a multifunctional probe designed with four tunable components including i) a Raman reporter as a barcoding component, ii) an antibody as a cancer cell detecting component, iii) a biotinylated double-stranded DNA (dsDNA) as a non-invasive isolating component, and iv) a gold nanoparticle as a Raman signal-enhancing component. In this demonstration, individually conjugated RANs are employed to detect both CCSCs and several major breast cancer CTC subtypes using five different surface markers: CD133, EpCAM, EGFR, HER2, and MUC1 (Fig. 1**a**). The CCSCs and CTCs are detected and isolated in an effective, selective, and noninvasive manner on the microfluidic chip *via* avidin-biotin reactions followed by restriction enzyme digestion of the dsDNA linker from the RANs (Fig. 1**b**). We have shown that selectively isolated CCSCs and CTCs successfully exhibit tumorigenicity and secondary tumor subtypes in both *in vitro and in vivo* model systems.

2. Materials and methods

2.1. Raman-active nanoprobe synthesis and characterization

In this work, we prepared five different combinations of RANs. Each type of RAN was conjugated with modification of a previously reported method by Qian et al. (2008). Fig. S1a shows the illustrations of the step-by-step conjugation process of the AuNP/Raman reporter/PEG/antibody/DNA conjugate. Briefly, RANs were prepared by adding a freshly prepared 1–5 μM Raman reporter solution dropwise to a rapidly mixing gold colloid at a 1:6 reporter solution and 60 nm AuNP colloid (BBI solutions EM.GC60, Cardiff, UK) volume ratio. Considering that each Raman reporter shows different signal enhancement effects with AuNPs, the concentration of reporters was determined from the signal to noise (S/N) ratio of the representative peak for each RAN. Concentrations of different Raman reporters (Thiophenol (TP, Sigma-Aldrich 240249), Nile Blue A (NBA, Sigma-Aldrich N0766), 1-naphthalenethiol (NPT, Sigma-Aldrich 724742), 4-mercaptopyridine (MPD, Sigma-Aldrich 148202), 2-quinolinethiol (QNT, Sigma-Aldrich

Table 1
Classification of breast cancer based on pathological features. Depends on the surface marker expression profiles, the subtype of breast cancer was categorized.

Subtype	Surface marker expression profile					Reference
	CD133	HER2	EGFR	EpCAM	MUC1	
Cancer Stem Cells	+					(Jordan et al., 2006; Medema, 2013; Visvader and Lindeman, 2008)
Luminal type	–			+		(Carey et al., 2007; Kao et al., 2009; Neve et al., 2006)
HER2 positive type		+			–	(Carey et al., 2007; Kao et al., 2009; Neve et al., 2006)
Basal-A type		–	+	–	+	(Carey et al., 2007; Kao et al., 2009; Neve et al., 2006)
Basal-B type	–	–	+	–	–	(Carey et al., 2007; Kao et al., 2009; Neve et al., 2006)

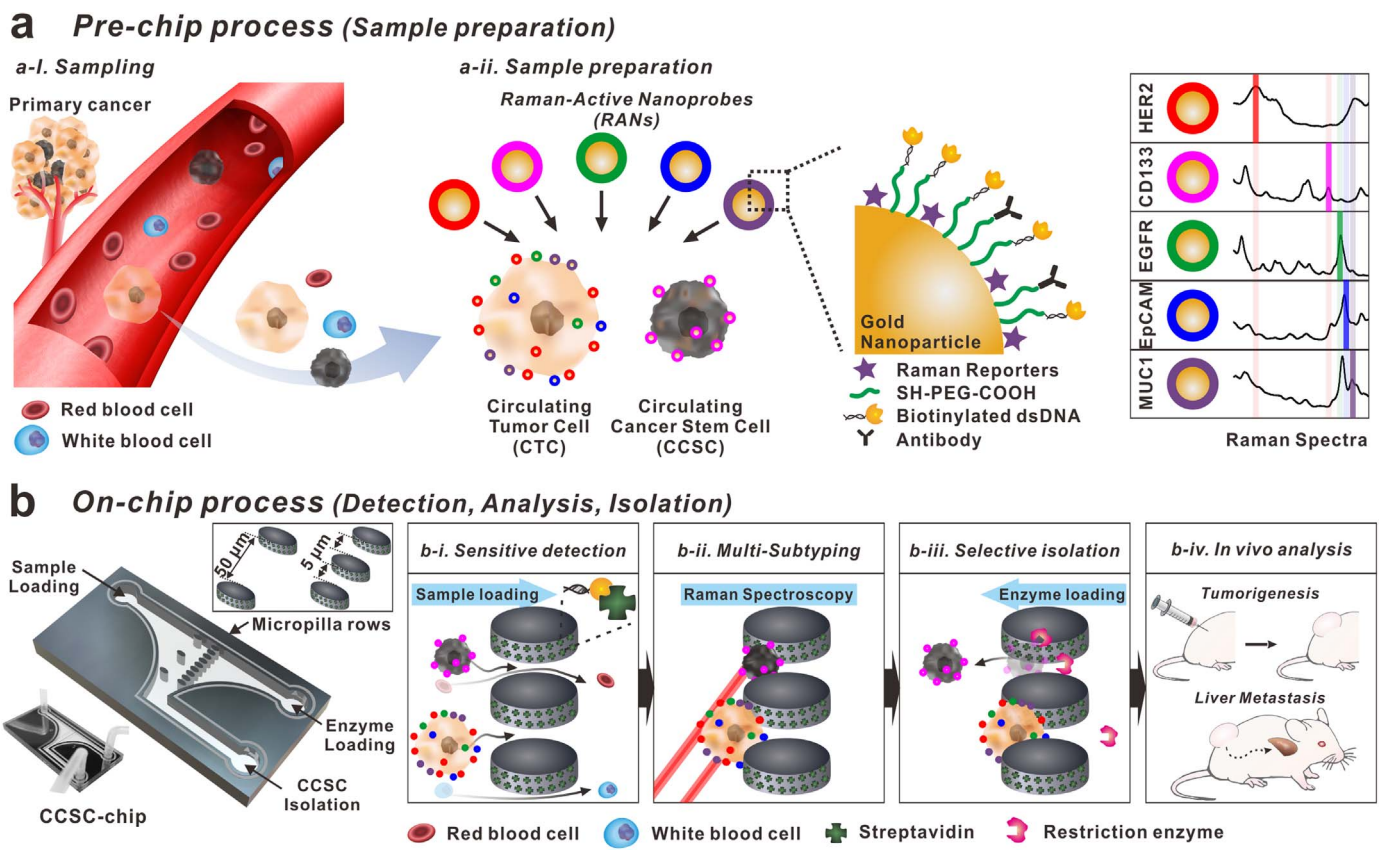

Fig. 1. Selective detection and analysis of cancer stem cell for monitoring tumorigenesis and metastasis. (**a**) The blood sample was prepared for chip-based analysis system. (**a-i**) Sampling the blood sample which contained circulating cancer stem cells (CCSCs) and circulating tumor cells (CTCs). (**a-ii**) The CCSCs and CTCs in blood sample were labeled with five types of multifunctional RANs; i) specific Raman reporter for signaling, ii) antibody for specific cell targeting and iii) biotinylated dsDNA for non-invasive isolation from the chip. (**b**) Blood sample solutions with RANs labeled CCSCs and CTCs were injected into the CCSC-chip and analyzed with a 3-step process on the chip; (**b-i**) Detection of RANs labeled CCSCs and CTCs by biotin-avidin interaction on streptavidin-coated micropillar, (**b-ii**) *In situ* subtyping of detected CCSC and CTC by Raman barcoding system, and (**b-iii**) Selective isolation of detected cells as two groups (CCSCs and CTCs) from the chip by using restriction enzyme. (**b-iv**) *In vivo* analysis to confirm the tumorigenicity, metastatic properties and secondary tumor subtypes of CCSCs.

116270)) were used in the following order, TP: 2 μM, NPT: 0.5 μM, MPD: 0.5 μM, QNT: 2 μM, and NBA: 4 μM as final concentration. After 10 min, 293 μl of 1 μM hetero-functional linker thiol-PEG-carboxyl (Sigma-Aldrich 757837) was added dropwise to a 3 ml Raman-encoded Au colloidal solution in a polypropylene tube under rapid mixing. After 15 min of vigorous mixing, the AuNPs were exposed to a large volume of PEG-thiol (Sigma-Aldrich 729108, 1.6 ml at 10 mM) to backfill the nanoparticle surface not covered by the hetero-functionalized PEG, yielding well-shielded and stable particle surfaces. Before covalent ligand conjugation at the carboxylic acid groups, the AuNPs were purified by three rounds of centrifugation (4000 rpm, 10 min) and re-suspension in PBS. To activate the carboxyl groups on the particle surface for covalent conjugation, freshly prepared ethyl dimethylaminopropyl carbodiimide (EDC) solution (5 ml, 40 mg/ml, Sigma-Aldrich E6383) and N-hydroxysulfosuccinimide sodium salt (sulfo-NHS, 5 ml, 110 mg/ml, Sigma-Aldrich 56485) were mixed vigorously at 25 °C for 15 min. Excess EDC and sulfo-NHS were separated from the activated nanoparticles by three rounds of centrifugation (4000 rpm, 10 min) and re-suspended in PBS. The purified AuNPs with activated carboxyl groups were then reacted with the mouse monoclonal antibodies (anti-CD133 (EMD Millipore MAB4399), anti-EpCAM (R&D systems MAB9601), anti-EGFR (R&D systems MAB1095), anti-HER2 (R&D systems MAB1192), and anti-MUC1 (AbFrontier YF-MA14321), 11.2 nmol) and H_2N-dsDNA-biotin (20 nmol, Bioneer, Daejeon, Korea) at 25 °C for 2 h, and the reaction mixture was stored at 4 °C for overnight. Excess antibody and DNA was removed by three rounds of centrifugation (4000 rpm, 10 min) and re-suspended in PBS.

Five different multifunctional RANs were prepared with five different combinations. The fully functionalized RANs were characterized by transmission electron microscopy (TEM), UV–vis spectroscopy, DLS, and SERS. UV–vis spectra were measured using Jasco V-530 UV/VIS spectrophotometer. The TEM images were acquired by using a JEOL transmission electron microscope (JEM1010) with an accelerating voltage of 80 kV at National Instrumentation Center for Environmental Management (NICEM, Seoul, Korea).

2.2. Design and fabrication of CCSC-chip

The CCSC-chip was designed with the rows of micropillars with different gap distances (5 and 50 μm) in a microfluidic channel. The cell containing solution will flow through the 50 μm and 5 μm gaps. When the solution passes the first micropillar row (50 μm gap), the microfluidic channel will generate the turbulent flow, which will help disperse the floating cells. The floating cells will then be filtered and trapped by the second 5 μm gap micropillar row by size, allowing the RBCs to pass (Fig. S2). The height of the microfluidic channel is 50 μm, with an intended design to minimize the vertical stacking of cells in a single 5 μm micro-pillar gap.

The CCSC-chip was fabricated by silicon-on-glass technology with a modified chip design from our previous study (Lee et al., 2013a). After the fabrication of the CCSC-chip, streptavidin was coated onto the micro-pillars surface by the following method. Briefly, the chips were sequentially rinsed with ethanol and deionized (DI) water and dried at 60 °C overnight. The chips were then placed in a plasma chamber (Convance-MP, Femto Science, Gyeonggi-do, Korea) and exposed to oxygen plasma (5 min) to activate surface silanols for the subsequent

reaction. The chips were sequentially immersed in a 10% 3-aminopropyltriethoxysilane (APTES) solution (Sigma-Aldrich A3648), thoroughly washed with DI water, and baked at 110 °C for 1 h. The silanized chips were exposed to 2% glutaraldehyde solution (Sigma-Aldrich G5882) in 100 mM phosphate buffer (pH 8.0) for 1 h, washed with PBS, and dried with nitrogen gas. 10 μM of streptavidin (Sigma-Aldrich S0677) was allowed to react with immobilized glutaraldehyde at room temperature (1 h). After washing with PBS, the chips were covered with 1% bovine serum albumin (Sigma-Aldrich A2153) in PBS (1 h) to block any sites that proteins did not bind to on the glutaraldehyde modified surface. Finally, the chips were washed with PBS solution and dried with nitrogen gas.

2.3. Cell culture and preparation of cell suspension solution

Three human breast cancer cell lines (Korea Cell Line Bank (KCLB) 30022), MDA-MB-231 (KCLB 30026) and SK-BR-3 (KCLB 30030)) were obtained from KCLB (Seoul, Korea). MCF-7, MDA-MB-231, and SK-BR-3 cell lines were grown in Roswell Park Memorial Institute (RPMI) 1640 (ThermoFisher Scientific 11875-093). All media were supplemented with 10% fetal bovine serum (FBS, Biowest S1520- 500) and 1% Penicillin-Streptomycin (ThermoFisher Scientific 15140163). Human breast CSC line and culture media were purchased from Celprogen (36102-29, Torrance, CA, USA). CSCs were cultured with maintenance media (Celprogen M36102-29S) to stabilize as an undifferentiated condition. Every cell line was grown in tissue culture plates (BD Biosciences, San Jose, CA, USA) in a 37 °C humidified incubator with 5% CO_2. At 80% confluence, the breast cancer cells were subcultured at a density of 1×10^5 cells/ml and the breast CSCs at 1×10^6 cells/ml on tissue culture plates, and the media were replaced every 3 days for the three breast cancer cell lines and every 2 days for CSCs.

48 h after sub-culturing, the cells were detached from the tissue culture plates using trypsin (ThermoFisher Scientific 25300054), after which it was washed twice with respective media to remove the detaching agent, trypsin. The cell pellets were re-suspended in the respective media and the number of cells were counted with a hemocytometer. The concentration of each suspended cell solution was matched as 1×10^4 cells/ml for next use.

2.4. Handling of healthy human blood

All healthy human blood samples were kindly donated from healthy donors through the Korea University (Seoul, Korea) with informed consent under an Institutional Review Board (IRB)-approved research protocol. The blood samples were collected using BD Vacutainer® CPT™ cell preparation tubes (BD 362753, Franklin Lakes, NJ, USA) containing sodium heparin and polyester gel. After gentle mixing, 4 ml of fresh blood was gently diluted twice with PBS. According to the literature, CCSCs and CTCs were present in the buffy coat layer with WBCs, therefore, we used a density gradient reagent (Ficoll-Paque plus, GE Healthcare 17–1440-02, Pittsburgh, PA, USA) to get the WBCs contained buffy coat. In a centrifuge tube, 6 ml of Ficoll-Paque plus was added followed by carefully adding but not mixing 8 ml of diluted blood and centrifugation at room temperature for 30 min at 400*g*. After centrifugation, the plasma layer was removed carefully from the top, and the low-density buffy coat cell layer containing lymphocytes and monocytes was collected while leaving the Ficoll and RBC sediment in the centrifuge tube. After collection, the cells were transferred to a new tube, resuspended in 4 ml PBS, and stored at 4 °C for next use.

2.5. CCSCs and CTCs labeled with RNP and injected into CCSC-chip

100 suspended cells of each subtype (CCSC, MCF-7, SK-BR-3, and MDA-MB-231) were mixed with the WBC suspension solution and then incubated with 10 pM. RANs with constant and gentle mixing for 30 min at room temperature. Then, the RAN labeled-cells were washed three times and resuspended in 400 μl of fresh culture medium. The RAN labeled-cell suspensions (containing 100 labeled cells) were infused through the microfluidic channel at a flow rate 10 μl/min and incubated at room temperature for 20 min to immobilize on the chip surface. Then the chip was washed with fresh culture medium to remove the debris or unbound cells (Fig. S2).

2.6. Acquisition of SERS mapping image and data analysis

NTEGRA Spectra (AFM-Raman Spectrometer, NT-MDT, Russia) equipped with a liquid nitrogen-cooled CCD detector and an inverted optical microscope (Olympus IX71) was used for SERS mapping the cells. SERS mapping images were acquired by scanning 1024 points (32 × 32) using a 785 nm NIR laser with 3 mW and 3 s exposure time on the sample plane. The SERS data was analyzed using Nova software (NT-MDT). After extracting 8 points of Raman spectra from the detected CCSC or CTC, a S/N ratio was calculated for each spectrum and averaged. The noise signal was extracted from 8 points in the background (outside of cell area) of the detected cell's Raman map image.

2.7. DNA cleavage and release of CCSCs/CTCs

To evaluate the cleavage efficiency of DNA linkers, two restriction enzymes, *Hin*dIII (New England BioLabs R0104S) and *Bam*HI (New England BioLabs R0136S), were subsequently treated on the CCSCs/CTCs detected in CCSC-chip. Enzyme solutions (500 unit/ml in NE Buffer2, New England BioLabs B7002S) flowed into the chip at a flow rate of 30 μl/min for 20 min at 37 °C. Released CTCs and CCSCs were isolated in a conical tube and transferred to a tissue culture plate for enrichment and culturing.

2.8. CCSC differentiation

Approximately 10,000 CCSCs were seeded in the 12-well plates. After 2 days of cultivation to promote CCSC attachment, maintenance media was changed to human breast cancer stem cell differentiation media (Celprogen M36102-29DS, Torrance, CA, USA) to start differentiation of CCSC. Media was changed every 3 days during the differentiation.

2.9. In vivo tumorigenesis assay

To examine the tumorigenic and metastatic property of CCSC *in vivo*, 6-week-old BALB/c nude mice were purchased from RaonBio (Yongin-si, Korea) (control, n = 4; xenograft with CCSCs, n = 9; xenograft). All animals were acclimatized to the animal facility for at least 72 h prior to experimentation and maintained according to the Guide for the Care and Use of Laboratory Animals published by the NIH. Every animal experiment was conducted under an Institutional Animal Care and Use Committee (IACUC)-approved research protocol. The animals were housed in a barrier under high-efficiency particulate air (HEPA) filtration and provided with sterilized food and water *ad libitum*. The animal facility maintained 12 h light/dark cycles at room temperature 21 ± 2 °C with 30–40% humidity. Approximately 5.0×10^6 cells of CD133 positive cells and CD133 negative cells were mixed with 354234-matrigel (BD, San Jose, California, USA) and subcutaneously injected into the left and right side of flanks nearby each leg. Nine weeks after inoculation, the grafted tumor tissues and livers were dissected and embedded in Tissue-Tek 100% optimal cutting temperature compound (O.C.T., Sakura Finetek, USA). Then the fresh tissue was rapidly snap frozen by putting it into liquid nitrogen and stored in a −80 °C freezer until further analysis. Freshly cryopreserved tissues were sliced (6 μm thick) using a −25 °C ultra-microtome (Leica CM 3050S, Wetzlar, Germany). Each section was picked up on an adhesion microscope glass slide (Paul Mariendeld GmbH & Co. KG, Lauda-Königshofen, Germany) followed by the careful washing out of the

O.C.T compound, with PBS. The sections were incubated with 2 mM probe 1 for 2 h and covered with fluorescent slide cover glass. The fluorescence microscopy images were taken using a confocal laser scanning microscope (LSM 5 Exciter, and LSM 710, Carl-Zeiss, Oberko, Germany). The mice that died before the 9-week mark were not counted.

2.10. Statistical analysis

Statistical analyses were carried out using GraphPad Prism. Normality of distribution and homogeneity of variance were validated and the statistical significance between the means was calculated using unpaired Student's *t*-test or Mann-Whitney test when normality tests failed. All numerical data presented with mean ± s.e.m. $P < 0.05$ was considered statistically significant.

3. Results and discussion

3.1. Selective detection and analysis of CCSCs/CTCs using a combinatorial RAN-based CCSC-chip

To distinguish five different types of circulating breast cancer cells including the CCSCs and four subtypes of CTCs, five RAN families were synthesized (Fig. S1a). To construct our RAN, we first conjugated the Raman reporter onto the gold nanoparticles' (AuNPs) surface by pairing them with each antibody to enable the RANs to have unique spectral-molecular signatures (Table S1). After a short incubation, the AuNP surface was coated with a thiol-terminated polyethylene glycol (thiol-PEG-carboxyl) to improve the stability of the RANs and prevent their aggregation in complex biological solutions. Antibodies and double-stranded DNAs (NH_2-dsDNA-Biotin) were conjugated to the PEG-conjugated AuNPs through EDC-NHS reaction to target and detect CCSCs/CTCs. Two different sequences of dsDNAs (DNA-A for CTCs and DNA-B for CCSCs) were specifically designed to select and isolate CCSCs and CTCs, which would be cleaved with the presence of specific restriction enzymes (Fig. S3). Through dynamic light scattering (DLS) analysis, the hydrodynamic size of RANs was determined to be 91.3 ± 2.3 nm (n = 10) in diameter (Fig. S1b). This hydrodynamic size was corroborated by the calculated value (94.2 nm), with a consideration of the length of the linkers and antibodies. Surface functionalization of AuNP with Raman reporters did not show any effect on the size distribution and monodispersity of the nanoparticle constructs as supported by TEM imaging (Fig. S1c).

More specifically, five different organic chemicals were selected as Raman reporters which have an aromatic ring and a thiol or amine group in their structure such as 2-quinolinethiol (QNT), 4-mercaptopyridine (MPD), 1-naphthalenethiol (NPT), Nile Blue A (NBA), and thiophenol (TP). Each Raman reporters showed specific Raman spectra when they were individually self-assembled onto AuNPs surface. From each RAN, one specific Raman transition with high S/N ratio (S/N > 1) was selected (*e.g.,* 469 cm^{-1} for NBA-HER2, 985 cm^{-1} for QNT-CD133, 1051 cm^{-1} for NPT-EGFR, 1096 cm^{-1} for MPT-EpCAM, and 1142 cm^{-1} for TP-MUC1) to represent ON and OFF value for each cancer marker at the corresponding position without any overlap (Fig. 2**a and** S4**a**). Although the Raman scattering signal intensity was affected by the concentration of Raman reporters (Figs. S4**b-g**) and the number of RANs in the unit area (0.04 μm^2, Figs. S5**a-c**), S/N ratios were used to represent ON (S/N > 50) and OFF (S/N < 50) states, which proved to be highly sensitive (ON, RANs ≥ 8) (Fig. 2**b and** S5**d**). The ON/OFF signal combinations of the five RAN families were utilized as barcodes for the distinguishing of the specific characters of detected CCSCs/CTCs.

To test the detection efficiency of our CCSC-chip system, RAN constructs were mixed with four different subtypes of human breast cancer cells (CCSC, MCF-7 (luminal), MDA-MB-231 (basal-B), and SK-BR-3 (HER2 positive) (100 cells per each type)) in WBCs containing buffy coat solution. The total 1 ml of prepared sample was infused into the CCSC-chip and washed with respective cell culture media multiple times by a syringe pump at a flow rate of 10 μl/min (duration ~30 min). During the fluidic process, infused samples were mixed and filtered by two different gaps (50 and 5 μm distances) provided by micro-pillar lines (Fig. 1**b**). With the presence of the large gap (50 μm), the sample was dispersed thoroughly *via* turbulent flow and CTCs were then selectively detected at the smaller gap (5 μm) by streptavidin-biotin interactions. It should be noted that the surface of the 5 μm gap pillars was conjugated with streptavidin to detect biotin-conjugated RAN labeled cells selectively upon contact with the pillar (Fig. 2**c**). Furthermore, the gap was designed to be wide enough for residual red blood cells (RBCs) (*ca.* 2.5 μm thickness) to pass through with minimal nonspecific detection of WBCs (Alvankarian et al., 2013; Schmid-Schonbein et al., 1980) (Fig. S6). Moreover, CCSCs and CTCs are bigger than the gap between each pillar (5 μm), thus maximizing the detection efficiency. To minimize remaining WBCs packed on the chip, we flushed with phosphate buffer saline (PBS, pH 7.4) from the opposing direction as a washing process. Furthermore, we tested our system with different pillar gap distances and showed that the detection of CTCs and CCSCs was not based solely on filtration due to the small gap distance (Fig. S7). For this purpose, several chips with three different pillar gaps at 20, 30, and 40 μm, wider than every type of CTCs and CCSCs, were fabricated and tested under the same conditions described above (Lee et al., 2013a). Regardless of the difference in pillar gap, both RANs treated CCSCs and CTCs were successfully detected and selectively isolated by undergoing enzymatic reaction. These results proved that CCSCs/CTCs are detected through a streptavidin-biotin reaction between micro-pillars and RANs instead of a non-specific physical adsorption.

After the selective detection of CCSCs/CTCs, an *in situ* analysis of the detected cells was conducted through a surface-enhanced Raman scattering (SERS) mapping method to characterize CCSCs and the specific subtypes of CTCs (Fig. 2**b and c**). Differently labeled RANs could selectively bind to the cellular membrane depending on the expression level of the surface markers (CD133, HER2, EGFR, EpCAM, and MUC1), while the distribution of Raman signal transitions at the corresponding peak positions (985 cm^{-1}, 469 cm^{-1}, 1051 cm^{-1}, 1096 cm^{-1} and 1142 cm^{-1}, respectively) and intensity differences could be considered as barcode signals to represent ON and OFF values of each surface markers (Fig. 2**d**). Accordingly, the characteristic information of detected CCSCs/CTCs were clearly distinguished based on observed barcode signals. For example, the presence of the observed Raman signal at 985 cm^{-1} represented the expression of stem cell marker CD133 on the cell surface which specifically corresponds to CCSCs. Subsequently, high expression of HER2 (at 469 cm^{-1}), EGFR (at 1051 cm^{-1}), and EpCAM (at 1096 cm^{-1}) corresponded to HER2 positive (SK-BR-3), basal-B (MDA-MB-231), and luminal (MCF-7) breast cancer cells, respectively (Figs. S8 and S9). By comparing surface marker characteristics, the detection efficiency for each cell type was 82.8 ± 6.2%, 91.8 ± 3.2%, 86.7 ± 4.1%, and 93.7 ± 4.4% for CCSC, MCF-7, MDA-MB-231, and SK-BR-3, respectively (Fig. 2**e**). The differences among detection efficiencies could be related to the number of expressed surface marker proteins which can be targeted with RANs. Particularly interesting, a substantial increase (16 – 86.7%) in capture efficiency for MDA-MB-231 cells was observed when compared to other EpCAM based CTC detection platform even though it exhibits only 1700 binding sites (Maetzel et al., 2009; Nagrath et al., 2007; Park et al., 2017; Prang et al., 2005; Sieuwerts et al., 2009). These improvements were strongly associated with the multi-probe platform for the microfluidic chip. Moreover, the averaged detection efficiency of RAN platform proved to be higher (90.7% vs 87.5%) when compared to our previous multi-nanoprobe methods (Lee et al., 2013a, 2013b).

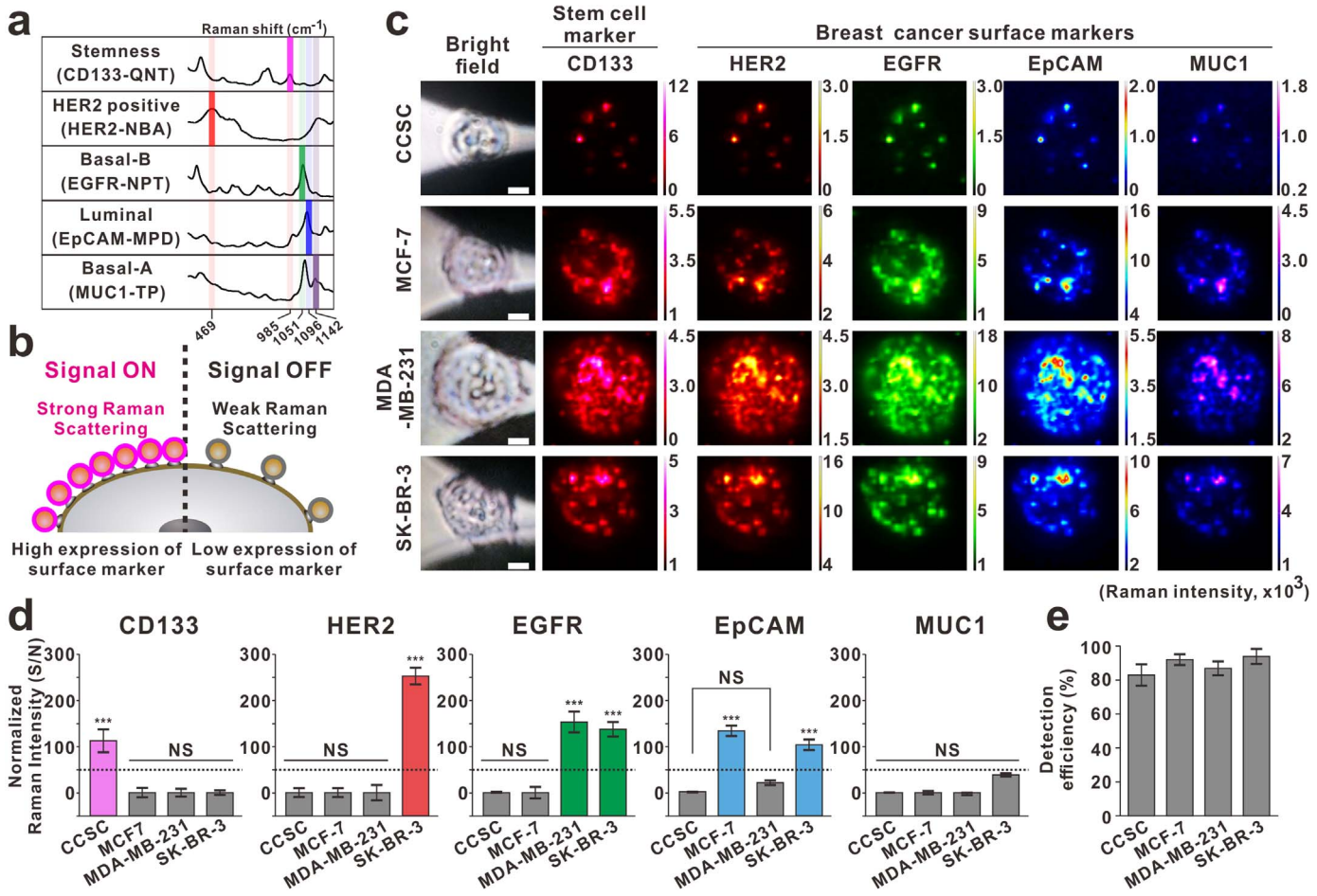

Fig. 2. Selective detection and analysis of living CCSCs/CTCs by RAN incorporated CCSC-chip. (**a**) The representative SERS peaks of five different types of RANs as barcoding system. Five different organic Raman reporters [Nile Blue A (NBA), 2-quinolinethiol (QNT), 1-naphthalenethiol (NPT), 4-mercaptopyridine (MPD), and thiophenol (TP)) are paired with each antibody to provide unique spectral-molecular signatures. From each RAN, one specific Raman peak with relatively high S/N ratios and little overlap with the other peaks was selected and assigned (469 cm^{-1} for NBA, 985 cm^{-1} for QNT, 1051 cm^{-1} for NPT, 1096 cm^{-1} for MPD, and 1142 cm^{-1} for TP) to represent ON and OFF values at corresponding position. (**b**) Schematic illustration of selective encoding of live CCSCs/CTCs by RANs based on expressed surface markers. (**c**) Optical microscope images and Raman maps obtained from detected CCSCs/CTCs. Raman maps were filtered with each RAN's representative peak (peak position ± 5 cm^{-1}) and pseudo-colored for easy recognition. Scale bar 4 μm. (**d**) The SERS barcoding pattern showed subtype specific information respectively. CCSC expressed stem cell marker CD133 only, MCF-7 expressed EpCAM only, MDA-MB-231 expressed EGFR only, and SK-BR-3 expressed HER2, EGFR and EpCAM (***P ≤ 0.001, relative to other markers). Dash line in the graph: threshold line (S/N = 50). (**e**) Detection efficiency of RAN labeled CCSC/CTCs on CCSC-chip showed 82.8%, 91.8%, 86.7%, and 93.7% for CCSC, MCF-7, MDA-MB-231, and SK-BR-3 respectively (n = 100). Experiments were repeated 3 times (n = 3) with 8 sampling points each. Values are given as mean ± s.e.m.

3.2. Selective and noninvasive isolation of CCSCs/CTCs for prediction of secondary tumor subtype

After on-chip analysis, detected CCSCs/CTCs were selectively isolated by utilizing two different restriction enzymes: *Hind*III and *Bam*HI (Fig. 3**a**). Since detected cells were bounded to the pillar by the streptavidin-biotin interaction with specific dsDNA sequences (DNA-A and DNA-B) serving as specific linkers between the biotin and RANs, CCSCs/CTCs were released in a selective and noninvasive manner by using the corresponding restriction enzymes sequentially (Fig. S3b). For example, to selectively isolate the CCSCs from CTCs, *Hind*III was first added, which cleaved the sequences of DNA-A that were targeted for EpCAM, EGFR, HER2, and MUC1 positives cells. Afterward, *Bam*HI was utilized to isolate CCSCs selectively. The optimal condition for the cleavage of both DNA linkers was identified to be 20 min with 500 unit/ml of restriction enzyme at 37 °C. This selective cleaving process for detected CCSCs and CTCs inside the chip was confirmed by the data shown in Fig. 3**a**. From this experiment, we demonstrated that the isolation efficiency for cell detection was 98.7 ± 1.2% and with a 93.0 ± 4.3% selectivity for CCSCs and 91.6 ± 5.8% selectivity for CTCs, after 5 times repetition. Surprisingly, the selectivity of the specific cell type isolation process was significantly improved (92.3% vs 66.7%) when compared to our previous report (Lee et al., 2013a). This improvement was associated with the surface marker expression profile of the CCSC and CTCs. Considering that CD133 is highly expressed on CCSCs, while other cancerous surface markers are barely expressed, CCSCs were labeled with one specific type of RAN which was conjugated with anti-CD133 antibody (Fig. S8).

More importantly, since the isolation process was done without comprising cell viability, we cultured the isolated CCSCs and controlled their differentiation to set up an *in vitro* model system to predict the subtype of metastatic derivatives. Without differentiation, cultured CCSCs demonstrated high expression of CD133-barcode of Raman spectra as expected and was further confirmed with fluorescence-activated cell sorting (FACS) (Figs. S10 and S11). As CCSCs were cultured in breast CSC differentiation media, a distinguishable change in the Raman spectra barcodes show a high expression of HER2 and EGFR instead of CD133 (stem cell marker), representing a HER2 positive breast cancer subtype (Fig. S11). These results indicate that the differentiation property of CCSCs was maintained even after a selective isolation process. Therefore, the isolated CCSCs could be utilized for *in vitro* metastatic cancer modeling as an indicator of a secondary tumor potential subtype (*e.g.* HER2 positive in this case). Note that *in vitro* cultured CCSCs were pretreated with RANs before SERS mapping.

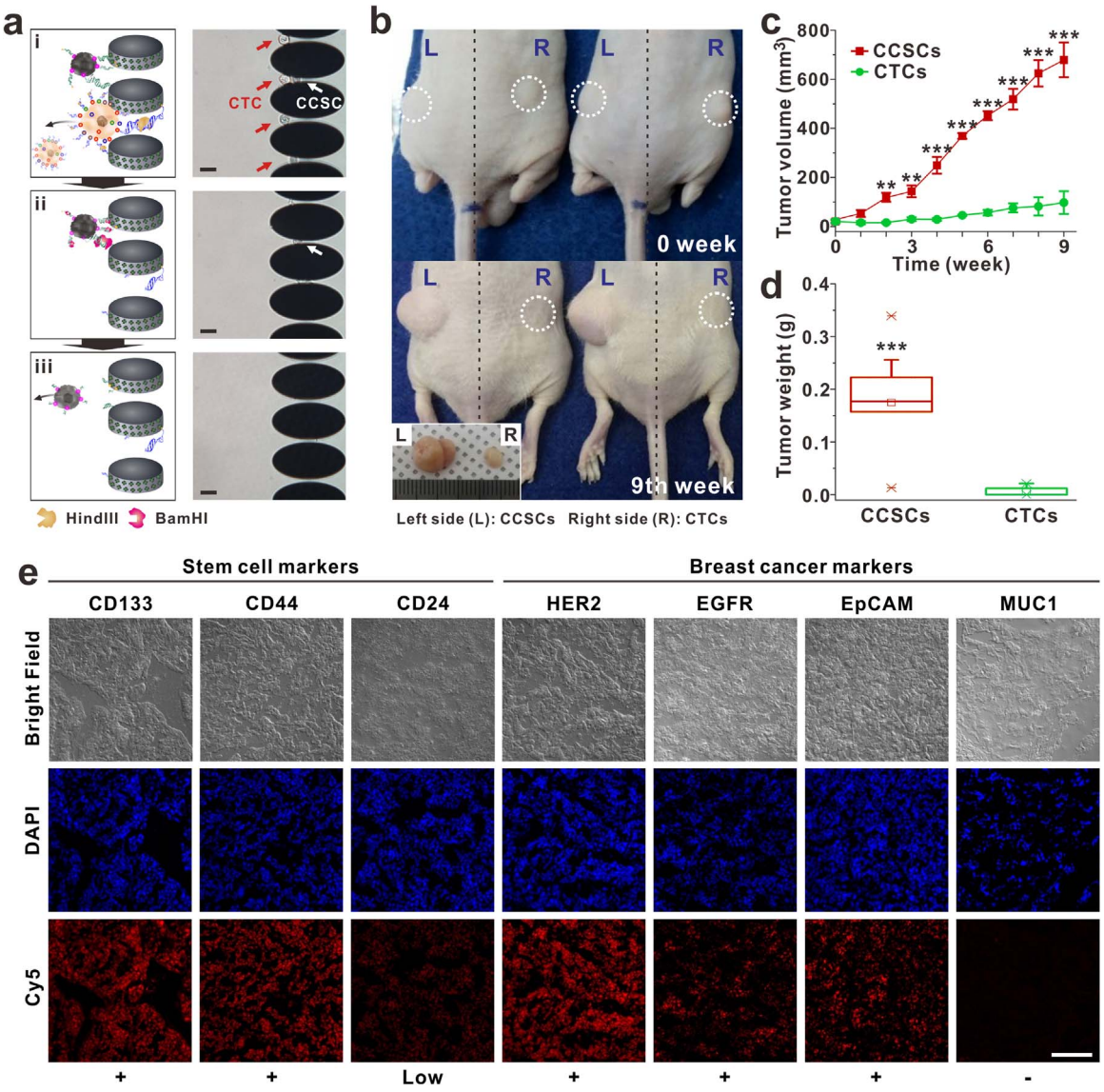

Fig. 3. *In vivo* tumorigenesis property of CCSCs and CTCs. (**a**) Schematic illustration and optical microscopy images of restriction enzyme-mediated selective cell retrieval process. (**a-i**) CCSC (white arrow) and CTCs (red arrows) were detected on pillar surfaces. (**a-ii**) *Hin*dIII was treated to cleave the dsDNA which conjugated with RAN-EpCAM, RAN-EGFR, RAN-MUC1, and RAN-HER2. After the washing step, every CTCs were successfully isolated except the CCSC. (**a-iii**) To isolate the remaining CCSC on a chip, *Bam*HI was treated. Each restriction enzymes treated for 30 min at 37 °C. Scale bar = 20 μm. (**b**) Selectively isolated CCSCs and CTCs were subcutaneously injected mice right after the injection (0 week) and 9th week (left side (L): CCSCs ($CD133^+$), right flank (R); CTCs ($CD133^-$)). The White circle indicates cell injected site. The inserted image showed extracted tumors from mice at 9th week (ruler: millimeter scale). (**c**) CCSCs showed significant tumorigenic property compare to CTCs. The size of the tumor was quantified at various time points. (**d**) Wet tissue weight of extracted tumor from each flank side of mouse 9 weeks after the cell injection. Data are means ± s.e.m. n = 9 (**0.001 < P ≤ 0.005, *** P ≤ 0.001, student's *t*-test), (**e**) Immunofluorescence image of surface markers expression in the tumor from CCSC injected site. Stem cell markers ($CD133^+$ and $CD44^+/CD24^{-/low}$) were still strongly expressed with HER2 expression. Scale bar = 100 μm.

Once *in vitro* confirmation was completed, the tumorigenic properties of the isolated CCSCs and stemless CTCs were further investigated using an *in vivo* animal model. Selectively isolated and expanded CCSCs and CTCs (5×10^5 cells each) were transplanted into male nude mice (n = 9) using subcutaneous injections at the left and right flank regions, respectively (Fig. 3**b**). We carefully selected a male nude mouse as a mouse model to prevent unexpected tumorigenesis caused by female mouse sex hormones (Caceres et al., 2016; Mohibi et al., 2011). After nine weeks, the tumor xenograft from the CCSCs injection site grew six times bigger in volume than the injection site of CTCs (Fig. 3**b and c**). The average size of the CCSC tumors was 10 mm in diameter with an average mass of 0.2 g, while tumors with stemless CTCs grew up to 3 mm with an average mass of 0.01 g (Fig. 3**d**). To conduct a more comprehensive study, the composition of the tumor developed by CCSCs was characterized by immunofluorescence staining of thin tumor slices (Fig. 3**e**). The immunostaining results of CCSC induced-tumor showed that the tumor cells were heterogeneous with a CSC population ($CD133^+$ and $CD44^+/CD24^{-/low}$) as well as different subtype specific breast cancers, including HER2 positive ($HER2^+$) and basal-B ($EGFR^+$, and $MUC1^-$), which were derived from CCSCs. This result further supported that transplanted CCSCs could proliferate as well as differentiate into subtype-specific cancer cells *in vivo*. Furthermore, since the *in vitro* biomarker expression patterns of differentiated CCSCs was quite similar with the *in vivo* results, we believe that an *in vitro* CCSC differentiation assay with our SERS-based barcode screening method can be utilized as an innovative tool for predicting secondary tumor compositions (Figs. S11 and 3**e**). Taken all together, noninvasively isolated CCSCs have great potential for advancing personalized medicine *via* identifying the heterogeneity of metastatic derivatives using both *in vitro* and *in vivo* cancer models.

In parallel, since we observed that CTCs could also generate tumors in an *in vivo* environment, the tumorigenic property of CTCs was investigated in detail. Three subtypes of breast cancer cells (MCF-7, MDA-MB-231, and SK-BR-3) and a normal breast epithelial cell line (human mammary epithelial cell, HMEC) (5×10^5 cells each) were implanted in male nude mice (n = 8) at both shoulders (left and right) and flank regions (left and right) (Fig. S12a). Nine weeks later, the injected MDA-MB-231 and MCF-7 cells generated a tumor at the injection site. Interestingly, SK-BR-3 and HMEC cells vanished two weeks post-injection and did not generate any tumors (Fig. S12b). However, MDA-MB-231 cells generated tumors larger (13 mm and 0.6 g) than the tumors generated by CCSCs. We speculated that this result might be due to the basal type cell line MDA-MB-231 showing a subpopulation of more than 90% $CD44^+/CD24^{-/low}$, which is indicative of prospective CSCs which have high tumorigenicity (Cheang et al., 2008; Fillmore and Kuperwasser, 2008; Karnoub et al., 2007). We also studied the metabolic abilities of injected CCSCs and CTCs. For this purpose, each subtype of cells was pre-cultured on an ultra-hydrophobic chamber (1×10^5 cells in 6 well-plate) to monitor the formation of spheroid shaped clusters. The spheroid formation was clearly observed from the CCSCs and MCF-7 cells, while MDA-MB-231 and SK-BR-3 cells could not generate spheroids (Fig. S13a). Indeed, “spheroids” or “sphere-forming cells” are commonly found in various solid tumor samples (ascites) and postulated as a key participant for *in vivo* tumorigenesis and metastasis (Leis et al., 2012; Wang et al., 2013). Moreover, we monitored the spreading speeds of CCSC and MCF-7 spheroids to confirm malignancy of the cancer cells for 21 h. The spreading speed of CCSC spheroid was dramatically faster than that of MCF-7 due to possible metabolic differences, which are known to affect the ability of cancer cells to survive, proliferate, and invade (Wiercinska et al., 2011) (Fig. S13b). Interestingly, the invasiveness of CCSC spheroid was improved in the three-dimensional environment conditions generated by a Matrigel block (Fig. S13c). Our results not only proved that CCSCs exhibit metabolic attributes that promote their ability to survive and generate a tumor *in vivo,* but also supports that the stem-like properties of CTCs are more critically related to secondary tumor formation. Lastly, the xenograft model of tumorigenesis was obtained from a fixed cell concentration (5×10^5 cells), hence tumorigenesis results could also vary for different cell concentration conditions.

3.3. Analysis of tumor metastasis risk by identifying CCSCs/CTCs

As a genuine metastatic cancer model system, blood samples (1.8 ml) were collected by cardiac puncture from xenograft models subjected to CCSCs and CTCs injections after clear tumor observation (Fig. 4). After incubating with RANs, 1.0 ml of RAN-labeled blood plasma was injected into our CCSC-chip with an optimized flow rate of 10 μl/min (Fig. 4**a**). Approximately 35 circulating epithelial cells were detected from both samples with a different distribution of Raman barcode signals observed (Fig. 4**b**). Both CCSCs and CTCs (HER2 positive) were detected from the CCSC injected xenograft model. On the other hand, in the various subtypes of mixed CTC injected xenograft models, only basal-B subtype CTCs were detected. Since the CCSCs and CTCs were observed from blood samples from animal disease models, we postulated that tumor metastasis was possible (Aceto et al., 2014; Baccelli et al., 2013). To verify the relationship between CCSC/CTC and tumor metastasis, liver tissues were extracted from the mouse model after euthanasia and tissue slices were generated as a standard model. Fluorescence images of thin liver sections (5 μm) showed remarkable expression of the anti-human CD133 marker (Cy3 labeled) in the liver, which was considered as direct evidence for the liver metastasis of the transplanted CCSCs (Fig. 4**c**). In particular, even though the total number of detected CCSCs and CTCs from each group were similar (negative = 18, positive = 19.25), the observed metastatic property was significantly different. Notably, when CCSCs were observed through the chip, a 100% rate of liver metastasis was observed while only 50% of liver metastasis was observed in the absence of CCSCs (Fig. 4**d**).

4. Conclusion

The advancement of precision medicine for the effective treatment of individual cancer patients essentially requires the development of an innovative method to detect CCSCs, as well as multiple CTC subtypes, with high sensitivity, to isolate their subpopulations selectively, and analyze their molecular features as well as their metastatic abilities in an accurate and non-invasive manner. To address the above challenges, here, we have demonstrated the selective detection and accurate analysis of the heterogeneous tumorigenic properties of CCSCs and CTCs by using a novel combinatorial RANs-based chip platform. Regarding the classification of breast cancer subtypes, basal type is considered as a triple-negative breast cancer due to a negative estrogen receptor (ER), progesterone receptor (PR), and HER2. The basal type expressing EGFR was further categorized into two subgroups; basal-A and basal-B. The expression of MUC1 was distinguished between basal-A (positive) and B (negative) (Kao et al., 2009). Accordingly, we chose MUC1 as a specific marker for basal-A and EGFR for basal-B (Kao et al., 2009). In this work, to cover the whole range of breast cancer subtypes and to confirm the stemness of CCSCs, we carefully designed five different RANs that can identify each CTC subtype and CCSC's stemness.

Furthermore, blood samples from either xenograft animal models or human patients can be mixed with our designed RANs to simultaneously detect, characterize, and isolate CCSCs and CTCs without compromising cell viability. Combinatorial RANs, each labeled with five Raman reporters, have unique Raman spectra which allow for distinguishing the five-different biomarker signals with minimum overlapping. Whole subtypes of breast CCSCs and CTCs were detected with *ca.* 90% efficiency and each cell subtype could be further characterized by Raman spectroscopy including luminal, HER2 positive, basal-A, and basal-B. The subtypes of breast cancers were known to have different functions and molecular characteristics in metastasis (Kennecke et al., 2010), population (Carey et al., 2006; Millikan et al., 2008), survival (Cheang et al., 2009; Cristofanilli et al., 2004; Hu et al., 2006; Perou et al., 2000; Sorlie et al., 2001), and response to treatment (Carey et al., 2007; Hugh et al., 2009; Nielsen et al., 2010; Prat et al., 2010). Furthermore, confirmation of CCSCs population in CTCs can provide a new insight into understanding a patient's metastatic status in detail. Although many clinical researchers have been investigating the prognostic relevance of CTCs in breast cancer and have suggested that CTCs can serve as valuable prognostic markers in all stages of breast cancer, the confirmation of CTC stemness, most relevant to the metastatic tumor type, has not been studied yet (Cristofanilli et al., 2004; Eroglu et al., 2013; Hayes et al., 2006; Janni et al., 2016; Pierga et al., 2008; Riethdorf et al., 2007). Therefore, our developed method will enable scientists to investigate the heterogeneous tumorigenicity of CTCs, which can then facilitate the study of chemotherapeutic effects on cancer metastasis, therefore improving the survival rate of cancer patients. Moreover, the differentiation profile of isolated CCSCs shows similar tumor subtypes in subcutaneously CCSC transplanted sites of the mouse model. This result illustrates that the analysis of differentiated CCSC can provide the subtype of the secondary tumor without conducting a biopsy.

In conclusion, our combinatorial RAN-based CCSC-chip will be valuable for a multi-detection system that can provide accurate cancer diagnosis and prognosis. Since CCSC marker in our method, CD133 (prominin-1), is widely believed to be a CSC marker in various solid tumor types such as breast (Nadal et al., 2013), colorectal (Lugli et al., 2010), brain (Singh et al., 2003), prostate (Collins et al., 2005), and lung cancer (Bertolini et al., 2009), the RAN-based CCSC-chip is able to apply for CCSC detection for other cancer types. We believe that our developed method is especially powerful for predicting tumor's metastatic capabilities through efficient CCSC/CTC detection, therefore, it

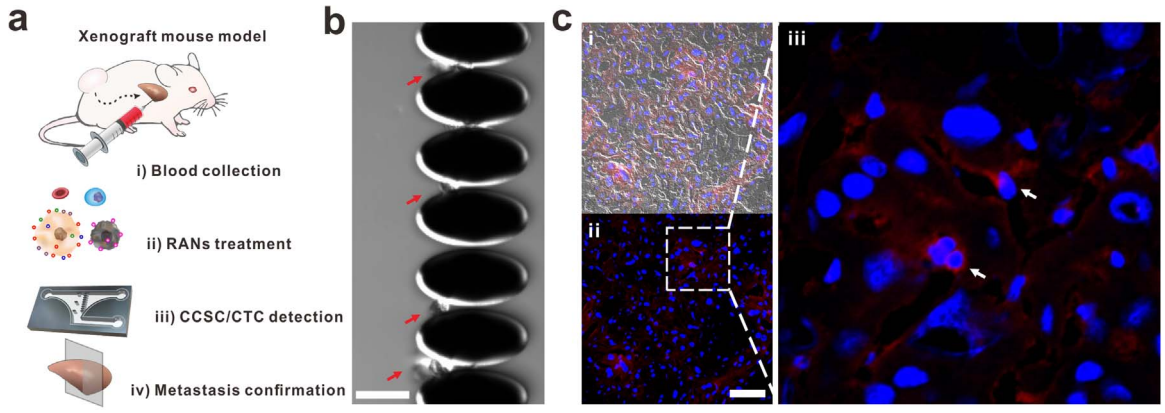

d

	Sample	Total number of captured cells	CCSCs ($CD133^+$)	CTCs ($CD133^-$)	Nonspecific bound cells	Liver metastasis
Tumor generated with CCSC injection	Mouse 1	11	3	5	3	O
	Mouse 2	27	5	21	1	O
	Mouse 3	22	7	13	2	O
	Mouse 4	17	3	10	4	O
Tumor generated with CTC injection	Mouse 1	13	-	11	2	X
	Mouse 2	32	-	28	4	O
	Mouse 3	24	-	21	3	O
	Mouse 4	3	-	2	1	X
Control	Mouse 1	-	-	-	-	X
	Mouse 2	-	-	-	-	X
	Mouse 3	-	-	-	-	X
	Mouse 4	-	-	-	-	X

Fig. 4. Relation between CCSCs/CTCs and Metastasis. (**a**) Schematic illustration of CCSC/CTC collection and confirmation of liver metastasis from a tumor containing mouse. Mouse blood was collected *via* cardiac punch after anathema. After labeling with RANs, CCSCs/CTCs in mouse blood sample were detected and analyzed on CCSC-chip. Right after the blood collection, liver tissue was extracted from the mouse and sliced for further analysis. (**b**) Detected CTCs and CCSCs from xenograft mouse blood. Scale bar, 50 μm. (**c**) Immunofluorescence image of liver tissue obtained from CSCC injected mouse for confirmation of metastasis. (**c-i**) Phase image of the liver tissue. CD133 was stained with Cy5, and nucleus was stained with DAPI. (**c-ii**) Fluorescence image of the liver tissue. (**c-iii**) Magnified image of (**c-ii**). The arrows indicate the overlapping fluorescence signal of the human CD133 positive cell and cell nucleus stained with DAPI. Scale bar, 10 μm. (**d**) Table showing the correlation between SCTC and metastasis. The 'CD133 positive ($CD133^+$) cell injection' group transplanted CCSC and CTC at left and right flank, and the 'CD133 negative ($CD133^-$) cell injection' group transplanted CD133 negative breast cells (MCF-7, MDA-MB-231, SK-BR-3, and HMEC) at both shoulder and hip joints. The mice died before 9-week mark were not counted. Scale bar: 50 μm.

can be tailored for precision medicine involving cancer metastasis prevention and the development of effective therapeutics against it.

Acknowledgements

J.-W.C. acknowledges financial support from the Leading Foreign Research Institute Recruitment Program, through the National Research Foundation of Korea (NRF), funded by the Ministry of Science, ICT and Future Planning (MSIP) (2013K1A4A3055268) and Basic Science Research Program through the National Research Foundation of Korea (NRF) funded by the Ministry of Education (2016R1A6A1A03012845). J.-H.K. acknowledges financial support from the Bio & Medical Technology Development Program of the NRF funded by the Korean government (2017M3A9B4042581).

Appendix A. Supplementary material

Supplementary data associated with this article can be found in the online version at http://dx.doi.org/10.1016/j.bios.2017.11.049.

References

Aceto, N., Bardia, A., Miyamoto, D.T., Donaldson, M.C., Wittner, B.S., Spencer, J.A., Yu, M., Pely, A., Engstrom, A., Zhu, H., Brannigan, B.W., Kapur, R., Stott, S.L., Shioda, T., Ramaswamy, S., Ting, D.T., Lin, C.P., Toner, M., Haber, D.A., Maheswaran, S., 2014. Circulating tumor cell clusters are oligoclonal precursors of breast cancer metastasis. Cell 158 (5), 1110–1122.

Al-Hajj, M., Wicha, M.S., Benito-Hernandez, A., Morrison, S.J., Clarke, M.F., 2003. Prospective identification of tumorigenic breast cancer cells. Proc. Natl. Acad. Sci. USA 100 (7), 3983–3988.

Alvankarian, J., Bahadorimehr, A., Yeop Majlis, B., 2013. A pillar-based microfilter for isolation of white blood cells on elastomeric substrate. Biomicrofluidics 7 (1), 14102.

Baccelli, I., Schneeweiss, A., Riethdorf, S., Stenzinger, A., Schillert, A., Vogel, V., Klein, C., Saini, M., Bauerle, T., Wallwiener, M., Holland-Letz, T., Hofner, T., Sprick, M., Scharpff, M., Marme, F., Sinn, H.P., Pantel, K., Weichert, W., Trumpp, A., 2013. Identification of a population of blood circulating tumor cells from breast cancer patients that initiates metastasis in a xenograft assay. Nat. Biotechnol. 31 (6), 539–544.

Bertolini, G., Roz, L., Perego, P., Tortoreto, M., Fontanella, E., Gatti, L., Pratesi, G., Fabbri, A., Andriani, F., Tinelli, S., Roz, E., Caserini, R., Lo Vullo, S., Camerini, T., Mariani, L., Delia, D., Calabro, E., Pastorino, U., Sozzi, G., 2009. Highly tumorigenic lung cancer CD133+ cells display stem-like features and are spared by cisplatin treatment. Proc. Natl. Acad. Sci. USA 106 (38), 16281–16286.

Caceres, S., Pena, L., Silvan, G., Illera, M.J., Woodward, W.A., Reuben, J.M., Illera, J.C., 2016. Steroid tumor environment in male and female mice model of canine and human inflammatory breast cancer. Biomed. Res. Int. 2016, 8909878.

Carey, L.A., Dees, E.C., Sawyer, L., Gatti, L., Moore, D.T., Collichio, F., Ollila, D.W., Sartor, C.I., Graham, M.L., Perou, C.M., 2007. The triple negative paradox: primary tumor chemosensitivity of breast cancer subtypes. Clin. Cancer Res. 13 (8), 2329–2334.

Carey, L.A., Perou, C.M., Livasy, C.A., Dressler, L.G., Cowan, D., Conway, K., Karaca, G., Troester, M.A., Tse, C.K., Edmiston, S., Deming, S.L., Geradts, J., Cheang, M.C., Nielsen, T.O., Moorman, P.G., Earp, H.S., Millikan, R.C., 2006. Race, breast cancer subtypes, and survival in the Carolina Breast Cancer Study. JAMA 295 (21), 2492–2502.

Cheang, M.C., Chia, S.K., Voduc, D., Gao, D., Leung, S., Snider, J., Watson, M., Davies, S., Bernard, P.S., Parker, J.S., Perou, C.M., Ellis, M.J., Nielsen, T.O., 2009. Ki67 index,

HER2 status, and prognosis of patients with luminal B breast cancer. J. Natl. Cancer Inst. 101 (10), 736–750.
Cheang, M.C., Voduc, D., Bajdik, C., Leung, S., McKinney, S., Chia, S.K., Perou, C.M., Nielsen, T.O., 2008. Basal-like breast cancer defined by five biomarkers has superior prognostic value than triple-negative phenotype. Clin. Cancer Res. 14 (5), 1368–1376.
Collins, A.T., Berry, P.A., Hyde, C., Stower, M.J., Maitland, N.J., 2005. Prospective identification of tumorigenic prostate cancer stem cells. Cancer Res. 65 (23), 10946–10951.
Cristofanilli, M., Budd, G.T., Ellis, M.J., Stopeck, A., Matera, J., Miller, M.C., Reuben, J.M., Doyle, G.V., Allard, W.J., Terstappen, L.W., Hayes, D.F., 2004. Circulating tumor cells, disease progression, and survival in metastatic breast cancer. N. Engl. J. Med. 351 (8), 781–791.
Eirew, P., Stingl, J., Raouf, A., Turashvili, G., Aparicio, S., Emerman, J.T., Eaves, C.J., 2008. A method for quantifying normal human mammary epithelial stem cells with in vivo regenerative ability. Nat. Med. 14 (12), 1384–1389.
Eroglu, Z., Fielder, O., Somlo, G., 2013. Analysis of circulating tumor cells in breast cancer. J. Natl. Compr. Cancer Netw. 11 (8), 977–985.
Fillmore, C.M., Kuperwasser, C., 2008. Human breast cancer cell lines contain stem-like cells that self-renew, give rise to phenotypically diverse progeny and survive chemotherapy. Breast Cancer Res. 10 (2), R25.
Ginestier, C., Hur, M.H., Charafe-Jauffret, E., Monville, F., Dutcher, J., Brown, M., Jacquemier, J., Viens, P., Kleer, C.G., Liu, S., Schott, A., Hayes, D., Birnbaum, D., Wicha, M.S., Dontu, G., 2007. ALDH1 is a marker of normal and malignant human mammary stem cells and a predictor of poor clinical outcome. Cell Stem Cell 1 (5), 555–567.
Hayes, D.F., Cristofanilli, M., Budd, G.T., Ellis, M.J., Stopeck, A., Miller, M.C., Matera, J., Allard, W.J., Doyle, G.V., Terstappen, L.W., 2006. Circulating tumor cells at each follow-up time point during therapy of metastatic breast cancer patients predict progression-free and overall survival. Clin. Cancer Res. 12 (14 Pt 1), 4218–4224.
Hu, Z., Fan, C., Oh, D.S., Marron, J.S., He, X., Qaqish, B.F., Livasy, C., Carey, L.A., Reynolds, E., Dressler, L., Nobel, A., Parker, J., Ewend, M.G., Sawyer, L.R., Wu, J., Liu, Y., Nanda, R., Tretiakova, M., Ruiz Orrico, A., Dreher, D., Palazzo, J.P., Perreard, L., Nelson, E., Mone, M., Hansen, H., Mullins, M., Quackenbush, J.F., Ellis, M.J., Olopade, O.I., Bernard, P.S., Perou, C.M., 2006. The molecular portraits of breast tumors are conserved across microarray platforms. BMC Genom. 7 (1), 96.
Hugh, J., Hanson, J., Cheang, M.C., Nielsen, T.O., Perou, C.M., Dumontet, C., Reed, J., Krajewska, M., Treilleux, I., Rupin, M., Magherini, E., Mackey, J., Martin, M., Vogel, C., 2009. Breast cancer subtypes and response to docetaxel in node-positive breast cancer: use of an immunohistochemical definition in the BCIRG 001 trial. J. Clin. Oncol. 27 (8), 1168–1176.
Janni, W.J., Rack, B., Terstappen, L.W., Pierga, J.Y., Taran, F.A., Fehm, T., Hall, C., de Groot, M.R., Bidard, F.C., Friedl, T.W., Fasching, P.A., Brucker, S.Y., Pantel, K., Lucci, A., 2016. Pooled analysis of the prognostic relevance of circulating tumor cells in primary breast cancer. Clin. Cancer Res. 22 (10), 2583–2593.
Jordan, C.T., Guzman, M.L., Noble, M., 2006. Cancer stem cells. N. Engl. J. Med. 355 (12), 1253–1261.
Kantara, C., O'Connell, M.R., Luthra, G., Gajjar, A., Sarkar, S., Ullrich, R.L., Singh, P., 2015. Methods for detecting circulating cancer stem cells (CCSCs) as a novel approach for diagnosis of colon cancer relapse/metastasis. Lab Invest. 95 (1), 100–112.
Kao, J., Salari, K., Bocanegra, M., Choi, Y.L., Girard, L., Gandhi, J., Kwei, K.A., Hernandez-Boussard, T., Wang, P., Gazdar, A.F., Minna, J.D., Pollack, J.R., 2009. Molecular profiling of breast cancer cell lines defines relevant tumor models and provides a resource for cancer gene discovery. PLoS One 4 (7), e6146.
Karnoub, A.E., Dash, A.B., Vo, A.P., Sullivan, A., Brooks, M.W., Bell, G.W., Richardson, A.L., Polyak, K., Tubo, R., Weinberg, R.A., 2007. Mesenchymal stem cells within tumour stroma promote breast cancer metastasis. Nature 449 (7162), 557–563.
Kennecke, H., Yerushalmi, R., Woods, R., Cheang, M.C., Voduc, D., Speers, C.H., Nielsen, T.O., Gelmon, K., 2010. Metastatic behavior of breast cancer subtypes. J. Clin. Oncol. 28 (20), 3271–3277.
Lawson, D.A., Bhakta, N.R., Kessenbrock, K., Prummel, K.D., Yu, Y., Takai, K., Zhou, A., Eyob, H., Balakrishnan, S., Wang, C.Y., Yaswen, P., Goga, A., Werb, Z., 2015. Single-cell analysis reveals a stem-cell program in human metastatic breast cancer cells. Nature 526 (7571), 131–135.
Lee, H.J., Cho, H.Y., Oh, J.H., Namkoong, K., Lee, J.G., Park, J.M., Lee, S.S., Huh, N., Choi, J.W., 2013a. Simultaneous capture and in situ analysis of circulating tumor cells using multiple hybrid nanoparticles. Biosens. Bioelectron. 47, 508–514.
Lee, H.J., Oh, J.H., Oh, J.M., Park, J.M., Lee, J.G., Kim, M.S., Kim, Y.J., Kang, H.J., Jeong, J., Kim, S.I., Lee, S.S., Choi, J.W., Huh, N., 2013b. Efficient isolation and accurate in situ analysis of circulating tumor cells using detachable beads and a high-pore-density filter. Angew. Chem. Int. Ed. Engl. 52 (32), 8337–8340.
Leis, O., Eguiara, A., Lopez-Arribillaga, E., Alberdi, M.J., Hernandez-Garcia, S., Elorriaga, K., Pandiella, A., Rezola, R., Martin, A.G., 2012. Sox2 expression in breast tumours and activation in breast cancer stem cells. Oncogene 31 (11), 1354–1365.
Lichtman, J.W., Conchello, J.A., 2005. Fluorescence microscopy. Nat. Methods 2 (12), 910–919.
Liu, S., Cong, Y., Wang, D., Sun, Y., Deng, L., Liu, Y., Martin-Trevino, R., Shang, L., McDermott, S.P., Landis, M.D., Hong, S., Adams, A., D'Angelo, R., Ginestier, C., Charafe-Jauffret, E., Clouthier, S.G., Birnbaum, D., Wong, S.T., Zhan, M., Chang, J.C., Wicha, M.S., 2014. Breast cancer stem cells transition between epithelial and mesenchymal states reflective of their normal counterparts. Stem Cell Rep. 2 (1), 78–91.
Lugli, A., Iezzi, G., Hostettler, I., Muraro, M.G., Mele, V., Tornillo, L., Carafa, V., Spagnoli, G., Terracciano, L., Zlobec, I., 2010. Prognostic impact of the expression of putative cancer stem cell markers CD133, CD166, CD44s, EpCAM, and ALDH1 in colorectal cancer. Br. J. Cancer 103 (3), 382–390.
Maetzel, D., Denzel, S., Mack, B., Canis, M., Went, P., Benk, M., Kieu, C., Papior, P., Baeuerle, P.A., Munz, M., Gires, O., 2009. Nuclear signalling by tumour-associated antigen EpCAM. Nat. Cell Biol. 11 (2), 162–171.
Maheswaran, S., Haber, D.A., 2010. Circulating tumor cells: a window into cancer biology and metastasis. Curr. Opin. Genet. Dev. 20 (1), 96–99.
Malanchi, I., Santamaria-Martinez, A., Susanto, E., Peng, H., Lehr, H.-A., Delaloye, J.-F., Huelsken, J., 2012. Interactions between cancer stem cells and their niche govern metastatic colonization. Nature 481 (7379), 85–89.
Medema, J.P., 2013. Cancer stem cells: the challenges ahead. Nat. Cell Biol. 15 (4), 338–344.
Melo, F.S., Kurtova, A.V., Harnoss, J.M., Kljavin, N., Hoeck, J.D., Hung, J., Anderson, J.E., Storm, E.E., Modrusan, Z., Koeppen, H., Dijkgraaf, G.J., Piskol, R., de Sauvage, F.J., 2017. A distinct role for Lgr5+ stem cells in primary and metastatic colon cancer. Nature 543 (7647), 676–680.
Millikan, R.C., Newman, B., Tse, C.K., Moorman, P.G., Conway, K., Dressler, L.G., Smith, L.V., Labbok, M.H., Geradts, J., Bensen, J.T., Jackson, S., Nyante, S., Livasy, C., Carey, L., Earp, H.S., Perou, C.M., 2008. Epidemiology of basal-like breast cancer. Breast Cancer Res. Treat. 109 (1), 123–139.
Mizrak, D., Brittan, M., Alison, M., 2008. CD133: molecule of the moment. J. Pathol. 214 (1), 3–9.
Mohibi, S., Mirza, S., Band, H., Band, V., 2011. Mouse models of estrogen receptor-positive breast cancer. J. Carcinog. 10 (1), 35.
Moncharmont, C., Levy, A., Gilormini, M., Bertrand, G., Chargari, C., Alphonse, G., Ardail, D., Rodriguez-Lafrasse, C., Magne, N., 2012. Targeting a cornerstone of radiation resistance: cancer stem cell. Cancer Lett. 322 (2), 139–147.
Nadal, R., Ortega, F.G., Salido, M., Lorente, J.A., Rodriguez-Rivera, M., Delgado-Rodriguez, M., Macia, M., Fernandez, A., Corominas, J.M., Garcia-Puche, J.L., Sanchez-Rovira, P., Sole, F., Serrano, M.J., 2013. CD133 expression in circulating tumor cells from breast cancer patients: potential role in resistance to chemotherapy. Int. J. Cancer 133 (10), 2398–2407.
Nagrath, S., Sequist, L.V., Maheswaran, S., Bell, D.W., Irimia, D., Ulkus, L., Smith, M.R., Kwak, E.L., Digumarthy, S., Muzikansky, A., Ryan, P., Balis, U.J., Tompkins, R.G., Haber, D.A., Toner, M., 2007. Isolation of rare circulating tumour cells in cancer patients by microchip technology. Nature 450 (7173), 1235–1239.
Neve, R.M., Chin, K., Fridlyand, J., Yeh, J., Baehner, F.L., Fevr, T., Clark, L., Bayani, N., Coppe, J.P., Tong, F., Speed, T., Spellman, P.T., DeVries, S., Lapuk, A., Wang, N.J., Kuo, W.L., Stilwell, J.L., Pinkel, D., Albertson, D.G., Waldman, F.M., McCormick, F., Dickson, R.B., Johnson, M.D., Lippman, M., Ethier, S., Gazdar, A., Gray, J.W., 2006. A collection of breast cancer cell lines for the study of functionally distinct cancer subtypes. Cancer Cell 10 (6), 515–527.
Nielsen, T.O., Parker, J.S., Leung, S., Voduc, D., Ebbert, M., Vickery, T., Davies, S.R., Snider, J., Stijleman, I.J., Reed, J., Cheang, M.C., Mardis, E.R., Perou, C.M., Bernard, P.S., Ellis, M.J., 2010. A comparison of PAM50 intrinsic subtyping with immunohistochemistry and clinical prognostic factors in tamoxifen-treated estrogen receptor-positive breast cancer. Clin. Cancer Res. 16 (21), 5222–5232.
Papadopoulou, E., Bell, S.E., 2011. Label-free detection of single-base mismatches in DNA by surface-enhanced Raman spectroscopy. Angew. Chem. Int. Ed. Engl. 50 (39), 9058–9061.
Park, M.H., Reategui, E., Li, W., Tessier, S.N., Wong, K.H., Jensen, A.E., Thapar, V., Ting, D., Toner, M., Stott, S.L., Hammond, P.T., 2017. Enhanced isolation and release of circulating tumor cells using nanoparticle binding and ligand exchange in a microfluidic chip. J. Am. Chem. Soc. 139 (7), 2741–2749.
Pathania, R., Kolhe, R.B., Ramachandran, S., Mariappan, G., Thakur, P., Prasad, P.D., Ganapathy, V., Thangaraju, M., 2016. Combination of DNMT and HDAC inhibitors reprogram cancer stem cell signaling to overcome drug resistance. Cancer Res. 76 (14 Supplement) (3325-3325).
Pattabiraman, D.R., Weinberg, R.A., 2014. Tackling the cancer stem cells—what challenges do they pose? Nat. Rev. Drug Discov. 13 (7), 497–512.
Perou, C.M., Sorlie, T., Eisen, M.B., van de Rijn, M., Jeffrey, S.S., Rees, C.A., Pollack, J.R., Ross, D.T., Johnsen, H., Akslen, L.A., Fluge, O., Pergamenschikov, A., Williams, C., Zhu, S.X., Lonning, P.E., Borresen-Dale, A.L., Brown, P.O., Botstein, D., 2000. Molecular portraits of human breast tumours. Nature 406 (6797), 747–752.
Pierga, J.Y., Bidard, F.C., Mathiot, C., Brain, E., Delaloge, S., Giachetti, S., de Cremoux, P., Salmon, R., Vincent-Salomon, A., Marty, M., 2008. Circulating tumor cell detection predicts early metastatic relapse after neoadjuvant chemotherapy in large operable and locally advanced breast cancer in a phase II randomized trial. Clin. Cancer Res. 14 (21), 7004–7010.
Prang, N., Preithner, S., Brischwein, K., Goster, P., Woppel, A., Muller, J., Steiger, C., Peters, M., Baeuerle, P.A., da Silva, A.J., 2005. Cellular and complement-dependent cytotoxicity of Ep-CAM-specific monoclonal antibody MT201 against breast cancer cell lines. Br. J. Cancer 92 (2), 342–349.
Prat, A., Parker, J.S., Karginova, O., Fan, C., Livasy, C., Herschkowitz, J.I., He, X., Perou, C.M., 2010. Phenotypic and molecular characterization of the claudin-low intrinsic subtype of breast cancer. Breast Cancer Res. 12 (5), R68.
Premasiri, W.R., Lee, J.C., Ziegler, L.D., 2012. Surface-enhanced Raman scattering of whole human blood, blood plasma, and red blood cells: cellular processes and bioanalytical sensing. J. Phys. Chem. B 116 (31), 9376–9386.
Qian, X., Peng, X.H., Ansari, D.O., Yin-Goen, Q., Chen, G.Z., Shin, D.M., Yang, L., Young, A.N., Wang, M.D., Nie, S., 2008. In vivo tumor targeting and spectroscopic detection with surface-enhanced Raman nanoparticle tags. Nat. Biotechnol. 26 (1), 83–90.
Riethdorf, S., Fritsche, H., Muller, V., Rau, T., Schindlbeck, C., Rack, B., Janni, W., Coith, C., Beck, K., Janicke, F., Jackson, S., Gornet, T., Cristofanilli, M., Pantel, K., 2007. Detection of circulating tumor cells in peripheral blood of patients with metastatic breast cancer: a validation study of the Cell Search system. Clin. Cancer Res. 13 (3), 920–928.
Riethdorf, S., Wikman, H., Pantel, K., 2008. Review: biological relevance of disseminated tumor cells in cancer patients. Int. J. Cancer 123 (9), 1991–2006.

Sabatte, G., Keir, R., Lawlor, M., Black, M., Graham, D., Smith, W.E., 2008. Comparison of surface-enhanced resonance Raman scattering and fluorescence for detection of a labeled antibody. Anal. Chem. 80 (7), 2351–2356.
Schmid-Schonbein, G.W., Shih, Y.Y., Chien, S., 1980. Morphometry of human leukocytes. Blood 56 (5), 866–875.
Sieuwerts, A.M., Kraan, J., Bolt, J., van der Spoel, P., Elstrodt, F., Schutte, M., Martens, J.W., Gratama, J.W., Sleijfer, S., Foekens, J.A., 2009. Anti-epithelial cell adhesion molecule antibodies and the detection of circulating normal-like breast tumor cells. J. Natl. Cancer Inst. 101 (1), 61–66.
Singh, S.K., Clarke, I.D., Terasaki, M., Bonn, V.E., Hawkins, C., Squire, J., Dirks, P.B., 2003. Identification of a cancer stem cell in human brain tumors. Cancer Res. 63 (18), 5821–5828.
Sorlie, T., Perou, C.M., Tibshirani, R., Aas, T., Geisler, S., Johnsen, H., Hastie, T., Eisen, M.B., van de Rijn, M., Jeffrey, S.S., Thorsen, T., Quist, H., Matese, J.C., Brown, P.O., Botstein, D., Lonning, P.E., Borresen-Dale, A.L., 2001. Gene expression patterns of breast carcinomas distinguish tumor subclasses with clinical implications. Proc. Natl. Acad. Sci. USA 98 (19), 10869–10874.
Visvader, J.E., Lindeman, G.J., 2008. Cancer stem cells in solid tumours: accumulating evidence and unresolved questions. Nat. Rev. Cancer 8 (10), 755–768.
Wang, X., Qian, X., Beitler, J.J., Chen, Z.G., Khuri, F.R., Lewis, M.M., Shin, H.J., Nie, S., Shin, D.M., 2011. Detection of circulating tumor cells in human peripheral blood using surface-enhanced Raman scattering nanoparticles. Cancer Res. 71 (5), 1526–1532.
Wang, Y.J., Bailey, J.M., Rovira, M., Leach, S.D., 2013. Sphere-forming assays for assessment of benign and malignant pancreatic stem cells. In: Su, H.G. (Ed.), Pancreatic Cancer: Methods and Protocols. Humana Press, Totowa, NJ, pp. 281–290.
Wiercinska, E., Naber, H.P., Pardali, E., van der Pluijm, G., van Dam, H., ten Dijke, P., 2011. The TGF-beta/Smad pathway induces breast cancer cell invasion through the up-regulation of matrix metalloproteinase 2 and 9 in a spheroid invasion model system. Breast Cancer Res. Treat. 128 (3), 657–666.
Ye, S., Li, X., Wang, M., Tang, B., 2017. Fluorescence and SERS imaging for the simultaneous absolute quantification of multiple miRNAs in living cells. Anal. Chem. 89 (9), 5124–5130.
Yoon, H.J., Kim, T.H., Zhang, Z., Azizi, E., Pham, T.M., Paoletti, C., Lin, J., Ramnath, N., Wicha, M.S., Hayes, D.F., Simeone, D.M., Nagrath, S., 2013. Sensitive capture of circulating tumour cells by functionalized graphene oxide nanosheets. Nat. Nanotechnol. 8 (10), 735–741.
Zhai, W.L., Li, D.W., Qu, L.L., Fossey, J.S., Long, Y.T., 2012. Multiple depositions of Ag nanoparticles on chemically modified agarose films for surface-enhanced Raman spectroscopy. Nanoscale 4 (1), 137–142.
Zhang, W., Lou, X., Meng, X., Zhu, L., 2016. Representation method for spectrally overlapping signals in flow cytometry based on fluorescence pulse time-delay estimation. Sensors 16 (11), 1978.
Zheng, J., Jiao, A., Yang, R., Li, H., Li, J., Shi, M., Ma, C., Jiang, Y., Deng, L., Tan, W., 2012. Fabricating a reversible and regenerable Raman-active substrate with a biomolecule-controlled DNA nanomachine. J. Am. Chem. Soc. 134 (49), 19957–19960.
Zöller, M., 2011. CD44: can a cancer-initiating cell profit from an abundantly expressed molecule? Nat. Rev. Cancer 11 (4), 254–267.